Real-Time Forecast of Dense Fog Events over Delhi: The Performance of the WRF Model during the WiFEX Field Campaign

PRAKASH PITHANI,[a,b] SACHIN D. GHUDE,[a] R. K. JENAMANI,[c] MRINAL BISWAS,[d] C. V. NAIDU,[b] SREYASHI DEBNATH,[a,e] RACHANA KULKARNI,[a,e] NARENDRA G. DHANGAR,[a] CHINMAY JENA,[a] ANUPAM HAZRA,[a] R. PHANI,[a] P. MUKHOPADHYAY,[a] THARA PRABHAKARAN,[a] RAVI S. NANJUNDIAH,[a,f] AND M. RAJEEVAN[g]

[a] *Indian Institute of Tropical Meteorology, Pune, India*
[b] *Department of Meteorology and Oceanography, Andhra University, Visakhapatnam, India*
[c] *India Meteorological Department, New ATC Building, IGI Airport, New Delhi, India*
[d] *National Center for Atmospheric Research, Boulder, Colorado*
[e] *Savitribai Phule Pune University, Pune, India*
[f] *Indian Institute of Science, Bangalore, India*
[g] *Ministry of Earth Sciences, New Delhi, India*

(Manuscript received 6 June 2019, in final form 29 January 2020)

ABSTRACT

A Winter Fog Experiment (WiFEX) was conducted to study the genesis of fog formation between winters 2016–17 and 2017–18 at Indira Gandhi International Airport (IGIA), Delhi, India. To support the WiFEX field campaign, the Weather Research and Forecasting (WRF) Model was used to produce real-time forecasts at 2-km horizontal grid spacing. This paper summarizes the performance of the model forecasts for 43 very dense fog episodes (visibility < 200 m) and preliminary evaluation of the model against the observations. Similarly, near-surface liquid water content (LWC) from models and continuous visibility observations are used as a metric for model evaluation. Results show that the skill score is relatively promising for the hit rate with a value of 0.78, whereas the false alarm rate (0.19) and missing rate (0.32) are quite low. This indicates that the model has reasonable predictive accuracy, and the performance of the real-time forecast is better for both dense fog events and no-fog events. For success cases, the model accurately captured the near-surface meteorological conditions, particularly the low-level moisture, wind fields, and temperature inversion. In contrast, for failed cases, the WRF Model shows large error in near-surface relative humidity and temperature compared to the observations, although it captures temperature inversions reasonably well. Our results also suggest that the model is able to capture the variability in fog onset for consecutive fog events. Errors in near-surface variables during failed cases are found to be affected by the errors in the initial conditions taken from the Indian Institute of Tropical Meteorology Global Forecasting System (IITM-GFS) spectral model forecast. Further evaluation of the operational forecasts for dense fog cases indicates that the error in predicting fog onset stage is relatively large (mean error of 4 h) compared to the dissipation stage.

1. Introduction

The northern part of India is considered to be one of the most fog-prone areas in the world during the winter season (December–January), where an extensive fog layer (from Pakistan to Bangladesh) can often be detected from the satellite images (Gautam et al. 2007; Jenamani 2012; Ghude et al. 2017). Formation of fog and its sustainment across the northern region of India is mainly dependent on the availability of moisture, stable atmospheric conditions, and strong low-level inversions, which mostly occur under the influence of a western disturbance (WD) (Pasricha et al. 2003; Dimri et al. 2015). The atmospheric aerosol can act as cloud condensation nuclei (CCN) and modify the life cycle of fog over Delhi (Ghude et al. 2017; Safai et al. 2019). Recent studies over India suggest an increase in frequency (both persistence and intensity) of fog from the past 10–15 years (Jenamani 2007; Syed et al. 2012).

Supplemental information related to this paper is available at the Journals Online website: https://doi.org/10.1175/WAF-D-19-0104.s1.

Corresponding author: Dr. Sachin Ghude, sachinghude@tropmet.res.in

DOI: 10.1175/WAF-D-19-0104.1

Some of the busiest airports (Delhi, Jaipur, Lucknow, and Varanasi), road, and rail networks in India are located in this region and get influenced by the fog episodes during the winter months (December–January). Aviation forecasters need timely information on dense fog hours to improve air-traffic management. It is especially essential for Indira Gandhi International Airport (IGIA) in Delhi because it is one of the busiest airports in India where around 70 flight operations (both takeoff and landing) occur per hour. Due to the impact of the fog, the total estimated economic loss to IGIA during 2011–16 was estimated at $3.9 million USD (Kulkarni et al. 2019). Therefore, fog prediction plays an essential role in road/rail transport, and for airline operations. There has been increasing concern in India to examine the genesis of fog formations and potential methods for operational fog forecasting on local to regional scales to mitigate the issue.

However, the accurate prediction of fog is very challenging for the present numerical weather prediction (NWP) models. This is mainly due to the complex processes involved in the fog formation, development, and dissipation (Gultepe et al. 2007, 2009; Gultepe 2015; Van der Velde et al. 2010; Steeneveld et al. 2015; Román-Cascón et al. 2016; Pithani et al. 2019a,b), which are not well represented. Prediction of fog has long been a challenge to the operational forecasters. Some efforts were made earlier using synoptic, statistical methods, and satellite images [India Meteorology Department (IMD) Science Plan 2010], a multirole-based diagnostic approach (Payra and Mohan 2014), an analog model (Goswami and Sarkar 2017), and a diagnostic approach (Bhowmik et al. 2004; Mitra et al. 2006) to predict fog in Delhi, but not in an operational forecasting setting. There have not been any studies in India to evaluate the accuracy of operational fog forecasts using a three-dimensional NWP model. Even though IMD is providing forecasts based on the coarser-resolution global and regional model, the skill of these forecasts is rather poor (IMD Fog Science Plan 2010). Therefore, to improve the NWP forecast skill, there is a need to understand complex interactions between the various atmospheric processes involved in fog formation. To address the key scientific needs and improve the wintertime fog prediction in India, the Ministry of Earth Sciences (MoES), Government of India (GoI) has initiated a multi-institutional research effort, the Winter Fog Experiment (WiFEX) at IGI Airport, New Delhi. The main aim of WiFEX is to understand the genesis of the fog, understand the limitations of the current NWP model, and develop a scientific tool for predictability of the fog for the northern region of India in general, and IGIA in particular. More details on the WiFEX can be found in Ghude et al. (2017).

During the WiFEX field campaign, a real-time forecast was conducted on experimental mode with Weather Research and Forecasting (WRF) Model for the winter 2016–17 and 2017–18. This forecast was also used to plan the intense observation periods (IOPs) during WiFEX. Several sensitivity experiments were conducted in hindcast mode to find out the best suite of physical parameterizations that show relatively better skill to predict the fog [in terms of liquid water content (LWC) and meteorological parameters] (Pithani et al. 2019a,b). In this paper, we explore the performance of the real-time WRF Model to forecast the dense fog [visibility (Vis) $<$ 200 m] events that occurred between 2016 and 2018 winter seasons at IGIA, New Delhi. WRF forecasts are compared with observations obtained during the field campaign to gain insight into the strengths (ability) and weaknesses of the WRF Model to predict the fog events, implications of the results, and open issues in model development have discussed in this article.

2. Model setup, the dataset used, and methodology

a. Model setup and for dataset for evaluation

A few recent studies have shown the ability of the WRF Model to predict reasonable near-surface variables during the fog conditions (Van der Velde et al. 2010; Steeneveld et al. 2015; Román-Cascón et al. 2016; Pithani et al. 2019a,b). Pithani et al. (2019a,b) have shown that the WRF Model could capture the entire life cycle of fog at two different sites in India. These studies showed promising results and led to the current operational configuration. The real-time operational forecasting system was set up using the WRF Model (version 3.6.1) in its nonhydrostatic configuration with a terrain-following vertical coordinate. The basic configuration setup for WRF is given in Table 1. The model setup uses a single domain with a horizontal grid resolution of 2 km centered on Delhi (28.49°N, 77.12°E) in the mercator conformal space with a grid dimension of 440 $\times$ 200 (Fig. 1). Based on the earlier sensitivity tests (Pithani et al. 2019b), the setup included 60 vertical levels with dense vertical levels below 1000 m (19 levels and 14 levels below 300 m) for detailed representations of the thermodynamical and surface processes within the planetary boundary layer (PBL). Multiple sensitivity experiments were carried out using a combination of different parameterization schemes (PBL, microphysics, land surface schemes), and model configuration (domain size and horizontal and vertical grid resolution) to determine the optimum configuration for predicting

TABLE 1. The WRF Model basic configuration used for this study.

WRF Model setup	Name of the scheme
Initial/boundary conditions (3 hourly)	IITM-GFS-T1534
Model domain size	440 × 200 grids
Domain resolution	2 km
Vertical resolution	60
Radiation scheme	CAM (shortwave and longwave)
Microphysics	WSM6
Land use land category	USGS+ISRO mixed over India
Land surface	Pleim–Xiu
PBL	MYNN2.5
Spin up	6 h

the dense fog events in India (Pithani et al. 2019a,b). Based on these earlier sensitivity tests, the physical parameterization schemes include the local turbulent kinetic energy (TKE) closure Mellor–Yamada–Nakanishi–Niño Level 2.5 (MYNN2.5) PBL scheme (Nakanishi and Niino 2006), WSM6 microphysics (Hong et al. 2006), CAM shortwave and longwave radiation scheme (Collins 2001a,b), and Pleim–Xiu land surface model (Gilliam and Pleim 2010). The WSM6 is a single-moment microphysics scheme; therefore, we have not changed the default cloud condensation number (CCN) concentration. To ensure more accurate surface conditions, default topography dataset with 30-s resolution derived from the 27 land use land categories of the U.S. Geological Survey (USGS) database was updated with Indian Space Research Organization (ISRO) land use dataset of 30-s resolution over India (Biswadip 2014; Pithani et al. 2019b). For the real-time forecast, the model was driven by the analysis and forecast product (ensemble Kalman filtering) produced by the Indian Institute of Tropical Meteorology Global Forecasting System (IITM-GFS, T1534) spectral model initial and boundary conditions at 12.5-km grid resolution (Mukhopadhyay et al. 2019). Daily 36-h forecasts were made with the initial time of 0000 UTC (0530 IST) during the whole period. Soil moisture from the GFS was interpolated to the model gird at two surface levels.

The real-time model forecasts were compared with the observations collected during the WiFEX campaign. Figure 2 shows the location of the experimental site (Fig. 2d) and in situ measurements (Figs. 2a–c) at IGIA, and Table 2 shows the observations used to evaluate the model forecast. These observations include hourly averaged measurements at the airport for visibility, the surface temperature at 2 m (T_2), 2-m relative humidity (Rh_2), 2-m specific humidity (Q_2), 10-m wind speed (Ws10), 10-m wind direction (Wd10), and radiosonde profiles launched at a distance 10 km away from the airport. In addition, we have also used observations of LWC derived from the fog-monitor (FM-120) instrument, turbulent kinetic energy (TKE), and friction velocity (u^*) estimated from the eddy covariance instrument for the events for which data were available. The detailed description of the experimental site and instruments used is presented in Ghude et al. (2017).

b. Methodology

Several fog cases were identified during winter 2016–17 and 2017–18 fog seasons over Delhi and were sampled by the measurements. Table 3 summarizes the number of fog events recorded (Vis < 200 m) during the study period. As per the International Civil Aviation Organization (ICAO) guidelines, takeoff and landing of aircraft under visual flight rules (VFR) are not allowed when the visibility is less than 500 m. These regulations are adjusted according to the experience of

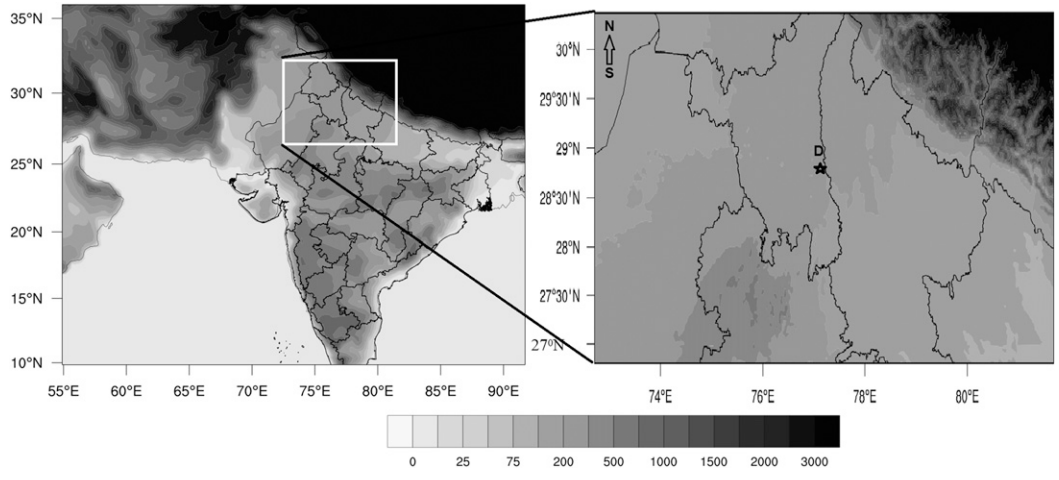

FIG. 1. (left) Topography map of the WRF Model simulation domain. (right) The WiFEX observational site is represented with a star symbol in a zoomed box of the model domain.

FIG. 2. (a) The 20-m flux tower installed at IGI Airport, New Delhi, (b) INSAT 3D satellite image showing a widespread fog layer over the Indo-Gangetic Plain (IGP; the square box represents the Delhi region), and (c) a Google map of the WiFEX campaign location inside IGI Airport (the star symbol represents the location of the flux tower).

the pilot, the type of aircraft, and the instrumentation at an airport and further classified as CAT-IIIA (Vis $<$ 300 m), CAT-IIIB (Vis $<$ 174 m), and CAT-IIIC (Vis $<$ 50 m) based on the visibility range. According to the AMS glossary, reduction of visibility below 1000 m due to suspension of water droplets near the surface is termed as a fog. In Delhi during winter months, the visibility drops below 1000 m on many days without any suspended water droplets in the air, mostly existing as haze. The fog droplet measurements during WiFEX show that usually smaller suspended droplets are recorded when visibility drops below 500 m. In the present study, dense

TABLE 2. In situ measurements used in this study for model comparison.

Type of instrument	Name	Parameters	Sampling
In situ sensor	Multicomponent weather sensor (GMX-500)	Temperature at 2 m	1 h
		Relative humidity at 2 m	1 h
		Wind speed at 10 m	1 h
In situ sensor for vertical profiles	Vaisala radiosonde	Temperature	1 min
		Relative humidity	1 min
In situ sensor for visibility	Runway visual range (RVR)	Visibility	1 m

TABLE 3. Summary of observed (visibility) and predicted (LWC) dense fog events during WiFEX 2016–17 and 2017–18 at IGI Airport, New Delhi. In the "total fog hours" column, "Y" is predicted fog events, "N" is failed fog events, and "F" is false alarm events.

		Total fog (Vis < 200 m)		
Station No.	Day	Onset lifting (UTC)	Total fog hours	Max LWC WRF (g m^{-3})
1	29–30 Nov 2016	0200–0400	2	0.24
2	30–1 Dec 2016	2200–0400	6	0.41
3	1–2 Dec 2016	1900–0500	10	—
4	6–7 Dec 2016	2000–0400	8	—
5	7–8 Dec 2016	1900–0100	6	—
6	10–11 Dec 2016	2300–0300	4	0.01
7	13–14 Dec 2016	0000–0200	3	—
8	23–24 Dec 2016	1900–0200	7	0.09
9	25–26 Dec 2016	1900–0300	8	0.06
10	26–27 Dec 2016	2200–0200	4	—
11	28–29 Dec 2016	—	—	0.05
12	29–30 Dec 2016	1800–2300	5	0.06
13	30–31 Dec 2016	1800–0200	8	0.20
14	31–1 Jan 2017	0000–0300	3	0.06
15	1–2 Jan 2017	0000–0200	2	0.20
16	2–3 Jan 2017	1800–0500	11	0.38
17	8–9 Jan 2017	0200–0500	3	0.006
18	15–16 Jan 2017	—	—	0.01
19	16–17 Jan 2017	2300–0200	3	—
20	17–18 Jan 2017	0100–0300	2	0.31
21	18–19 Jan 2017	2100–0300	6	0.01
22	19–20 Jan 2017	2100–0300	6	—
23	22–23 Jan 2017	1800–0400	10	0.06
24	27–28 Jan 2017	0000–0500	5	0.35
25	28–29 Jan 2017	2300–0200	3	0.22
26	29–30 Jan 2017	2000–0400	8	0.29
27	30–31 Jan 2017	2300–0200	3	0.51
28	31–1 Feb 2017	2300–0400	5	0.59
29	1–2 Feb 2017	2200–0200	4	0.65
30	5–6 Feb 2017	2300–0400	5	0.56
31	13–14 Dec 2017	1800–2200	4	—
32	30–31 Dec 2017	2300–0700	8	—
33	31–1 Jan 2018	2300–0300	4	—
34	1–2 Jan 2018	1300–2300	10	—
35	3–4 Jan 2018	1800–0600	12	0.009
36	5–6 Jan 2018	0000–0400	4	0.28
37	6–7 Jan 2018	2300–0400	5	—
38	11–12 Jan 2018	2300–0300	4	—
39	12–13 Jan 2018	1300–2300	10	—
40	14–15 Jan 2018	—	—	0.001
41	16–17 Jan 2018	—	—	0.18
42	18–19 Jan 2018	2300–0500	6	0.47
43	19–20 Jan 2018	1900–0800	13	—
44	22–23 Jan 2018	—	—	0.01
45	24–25 Jan 2018	2000–0300	7	0.33
46	25–26 Jan 2018	1900–0400	09	0.37
47	27–28 Jan 2018	2000–0500	09	0.61
48	28–29 Jan 2018	0000–0300	03	0.49
		260	29 (Y)/14 (N)/05 (F)	

fog is defined as an event when the visibility drops below 200 m for at least 2 h. For the safe flight operation at IGIA, it is necessary to forecast fog conditions occurring below a visibility of 200 m. Using this criterion, 40 moderate fog events (200 m < Vis < 500 m) and 43 dense fog events (Vis < 200 m) were recorded at IGIA during the 2016–17 and 2017–18 winter seasons. Considering the challenges associated with predicting onset and lifting of fog events, particularly for CAT-III conditions, fog events with Vis < 200 m are studied in detail. This paper, therefore, focuses on the evaluation of dense fog episodes, instead of all fog events, occurred

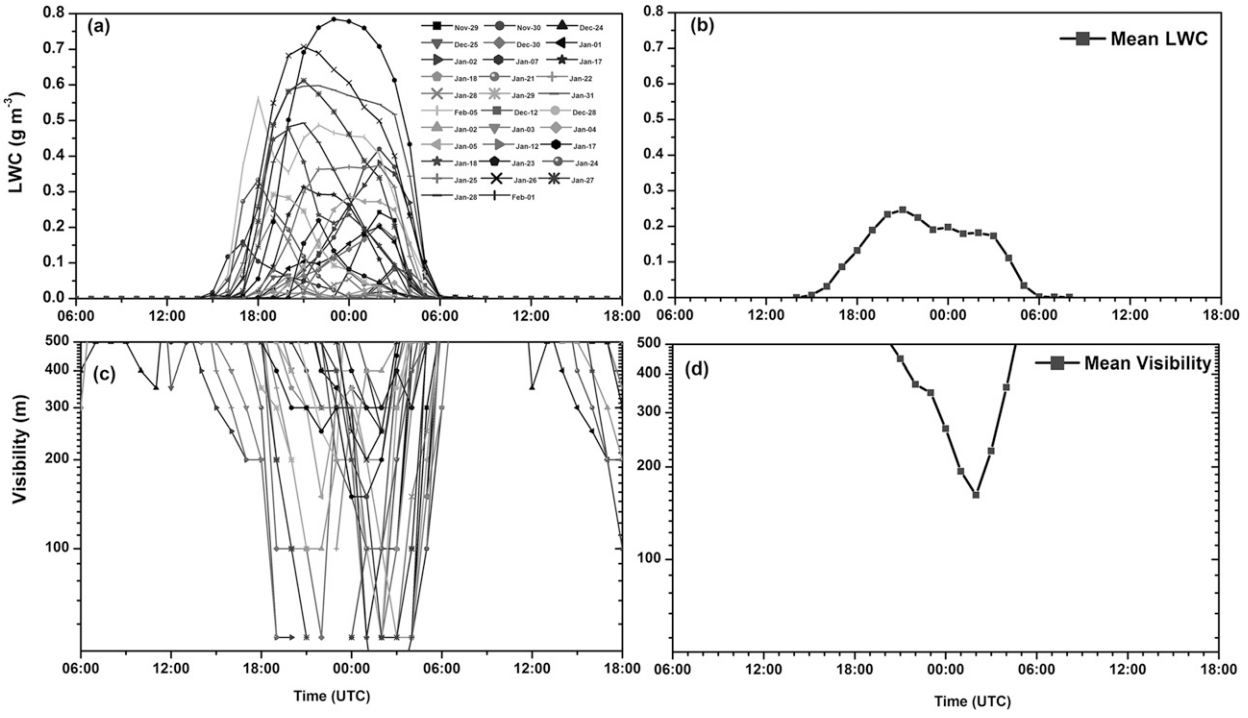

FIG. 3. Temporal evolution of (a) simulated LWC ($g\,m^{-3}$), (b) simulated mean LWC ($g\,m^{-3}$), (c) observed runway visibility (m) on different dense fog days, and (d) mean visibility (m) for all dense fog days.

at IGI airport. Table 3 summarizes different characteristics [onset (Vis < 200 m), duration (Vis < 200 m), maximum simulated LWC] of the dense fog events observed and simulated by the model during WiFEX 2016–17 and 2017–18 at the study location. We find the highest frequency of dense fog onset during early morning hours [between 0000 and 0300 UTC (0530–0730 IST)]; however, some dense fog events are occurring during midnight [~2200 UTC (0330 IST)], and few of them also happen before midnight [~1900 UTC (0030 IST)].

WRF has the ability to predict LWC, which directly represents low-level clouds and thus provides a good representation of fog (Zhou and Du 2010; Steeneveld et al. 2015). Analyzing LWC variations in near-surface model levels, life cycle, and the vertical and horizontal extent of the fog can be assessed (Pithani et al. 2019a,b). In the present study, fog predicted by the model is represented directly by the simulated LWC near the model surface level. To evaluate the model performance, simulated LWC near the surface at every hour was further compared with the hourly observations of visibility from the runway visual range (RVR) instrument. Figure 3 presents the temporal evolution of simulated LWC and observed visibility for all the predicted dense fog events. By examining the mean diurnal cycle of visibility reduction (Fig. 3d) during these fog events, it appears that the overall modeled LWC (Fig. 3c) follows the mean fog onset, sustainment, and dissipation stage of the fog life cycle. Further, LWC derived from the fog droplet spectrum measured by a fog monitor instrument (FM-120) was compared with the simulated LWC (Figs. 4b,c) for seven dense fog events for which LWC data were available. This instrument was operated during winter 2017–18 on a few intensive observation periods (IOPs). Hence, the observed LWC data were not available for all the 44 dense fog events. Interestingly, we find that modeled LWC followed the mean life cycle of observed LWC (Fig. 4c), but the predicted LWC was higher in magnitude during the onset and mature phase. This indicates that the important physical and thermodynamical parameters needed for the dense fog formation seems to be simulated reasonably well by the model. For the majority of fog events, the mean fog duration (Vis < 200 m) is about 2–5 h. However, each fog event (Fig. 3c) has specific onset timing, duration, and intensity, and was not evenly distributed throughout the period. The most long-lasting dense fog events (duration > 10 h) occurred on 2–3 January 2017 (11 h), 3–4 January 2018 (12 h), 19–20 January 2018 (13 h), and 25–26 January 2018 (19 h). The behavior of each of the dense fog events shows significant variability in the temporal distribution of fog onset, sustainment, and dissipation, and the model predicted LWC shows the ability to capture this variability to a

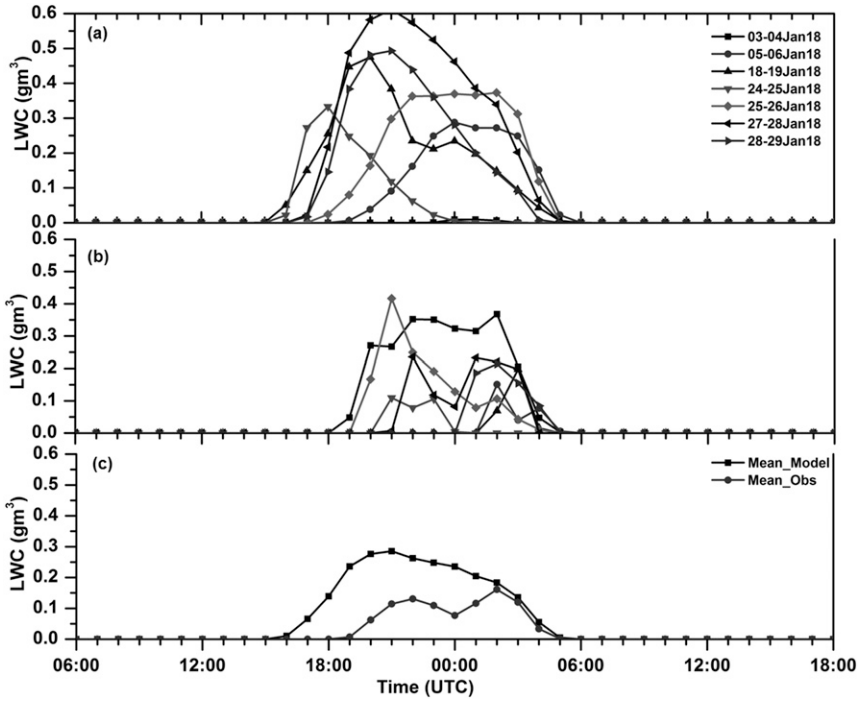

FIG. 4. Temporal evolution of (a) simulated LWC (g m^{-3}) and (b) observed LWC (g m^{-3}) for seven different dense fog events, and (c) comparison between simulated and observed mean LWC (g m^{-3}) during January 2018.

large extent (Fig. 3a). For example, Fig. S1 (in the online supplemental material) shows that the visibility on 29 November 2017 dropped below 500 m at around 2300 UTC (0430 IST), while dense fog conditions prevailed for almost 2.5 h. On the other hand, visibility recorded on 30 November 2017 indicates that the fog started (Vis $<$ 500 m) around 2000 UTC (0130 IST), 3 h earlier than the preceding day, and dense fog condition (Vis $<$ 200) prevailed for about 3.5 h. Interestingly, the evolution of LWC simulated by the model indicates fog onset around 2300 UTC (0430 IST) on 29 November and around 2000 UTC (0130 IST) on 30 November, which illustrates the ability of the WRF Model to capture the onset variability of fog events that occurred on consecutive days. The correlation ($r = 0.62$) between observed visibility and model predicted LWC for all dense fog events indicates that the WRF forecasting setup used in the present study has the reasonable predictive capability for dense fog events observed at IGI Airport, New Delhi, India.

3. Results

Performance of WRF during successful and failed cases

To examine the model performance for fog forecasting, one simulation each for the one successful, failed, and false alarm cases are evaluated. Subsequently, composites of the success and failed cases are scrutinized to assess the fog forecasting capability for dense fog events (presented in Table 3). Simulations are compared with the observations of T_2, Q_2, Ws10, Wd10, and radiosonde profiles of temperature and humidity. Since most of the current fog forecasts from NWP models use the model's lowest-level LWC for determining fog, it will be meaningful to compare how well the LWC forecast performs against the visibility observations.

1) SUCCESS FOR DENSE FOG EVENTS

Figures 5a and 5b show the observed visibility and simulated LWC, respectively, for the dense fog event that occurred over the IGI airport on the morning of 30 November 2016. Figure 6 shows the forecast for temperature (Fig. 6a), specific humidity (Fig. 6b) and humidity (Fig. 6b) profile at 0000 UTC (0530 IST) for the same event. The sounding showed a deeper inversion and vertically moist atmosphere extending from surface up to 200 m, which is indicative of favorable environmental conditions for the dense fog formation (Wærsted et al. 2019) and its maintenance at IGI Airport (Ghude et al. 2017). The real-time WRF forecast model was able to predict the observed strength of surface

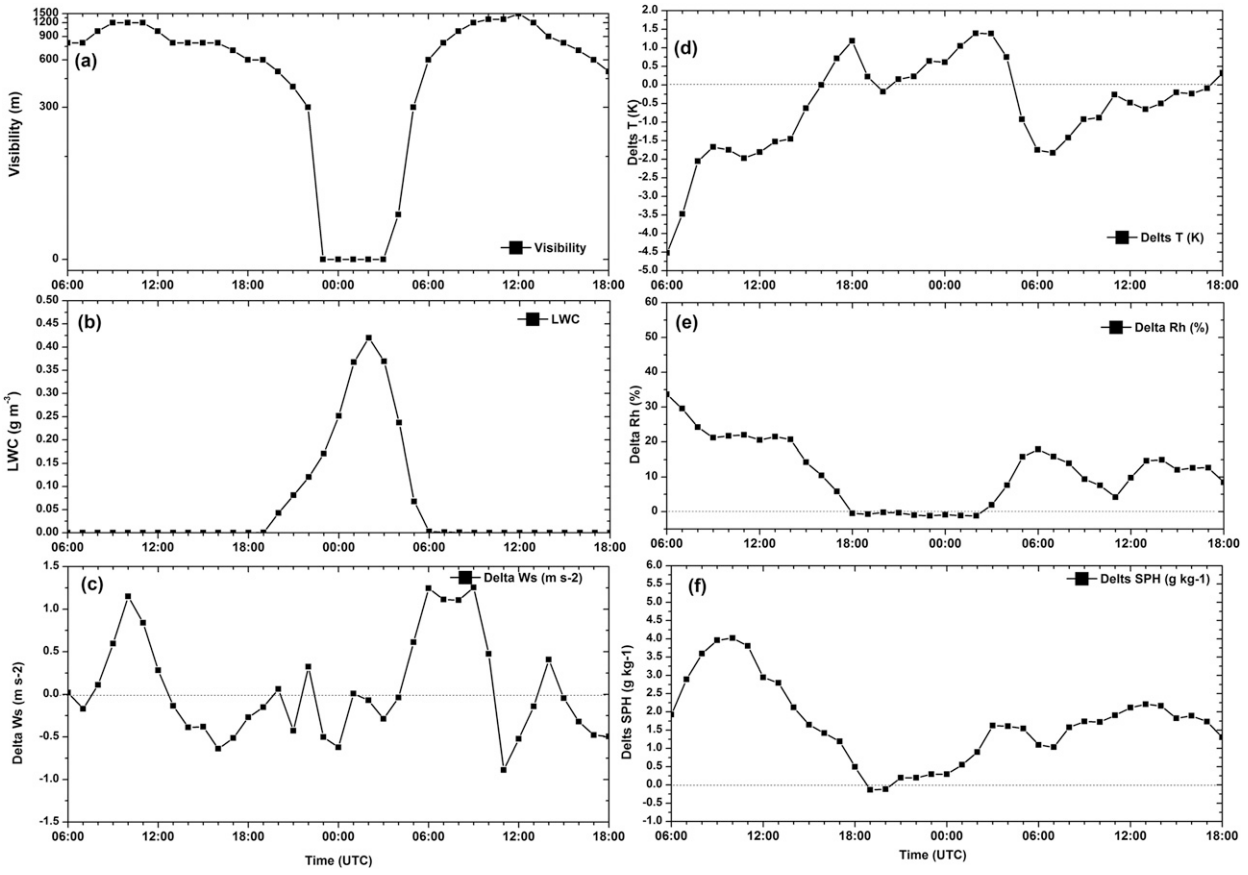

FIG. 5. (a) Time series of observed visibility (m), (b) simulated LWC ($g\,m^{-3}$), (c) the difference between observed and simulated (observed − simulated) wind speed at 10 m, (d) temperature at 2 m (T_2), (e) relative humidity at 2 m (Rh_2), and (f) specific humidity at 2 m (Q_2) during 29–30 Nov 2016.

inversion and vertical moisture structure closely, indicating that near-surface atmospheric conditions are simulated reasonably well during this event. Visibility evolution in Fig. 5a indicates that dense fog (Vis < 200 m) onset occurred at around 2200 UTC (0330 IST) and persisted for about 5 h. LWC produced by the model able to predict the onset and dissipation stage (Fig. 5b), capturing the entire fog cycle reasonably well. The difference between observed and simulated temperatures presented in Fig. 5d indicates that the simulations have successfully reproduced the surface temperature most consistently between evening and morning hours; however, we find that it is slightly overestimated (by about 0.8 K) during nighttime, which might cause enhance condensations and high LWC near the surface. The evolution of Ws10 (Fig. 5c), is in good agreement with the observations (Fig. 5c) between evening and morning hours. The difference between simulated and observed Rh_2 (Fig. 5e) and Q_2 (Fig. 5f) is close to zero, which illustrates that the model is able to capture most of the saturated surface conditions during the dense fog period (Figs. 5e,f). Overall, the model was able to capture the characteristics of the ideal meteorological variable to represent the fog accurately.

Composite of temperature and humidity profiles for the successful cases (Table 3) shown in Figs S3a and S3b further support this conclusion. These profiles represent prevailing atmospheric conditions simulated by the model during dense fog periods. We find that in most cases, real-time forecasts capture the temperature inversions and vertical moisture conditions, although they have some deviation in the strength and capping of the surface inversion. A composite of deviations between observed and forecasted T_2, Q_2, Ws10, and Wd10 is illustrated in Figs. 7a–d, respectively, for all the success fog events shown in Table 3. We find that the difference between observed and predicted T_2 was often less than 1 K compared to observations (slight cold bias) for most of the success cases, especially during late evening till early morning hours. Similarly, the difference between observed and predicted Q_2 was slightly higher ($0.1\,g\,kg^{-1}$). The model also simulates satisfactorily observed TKE and

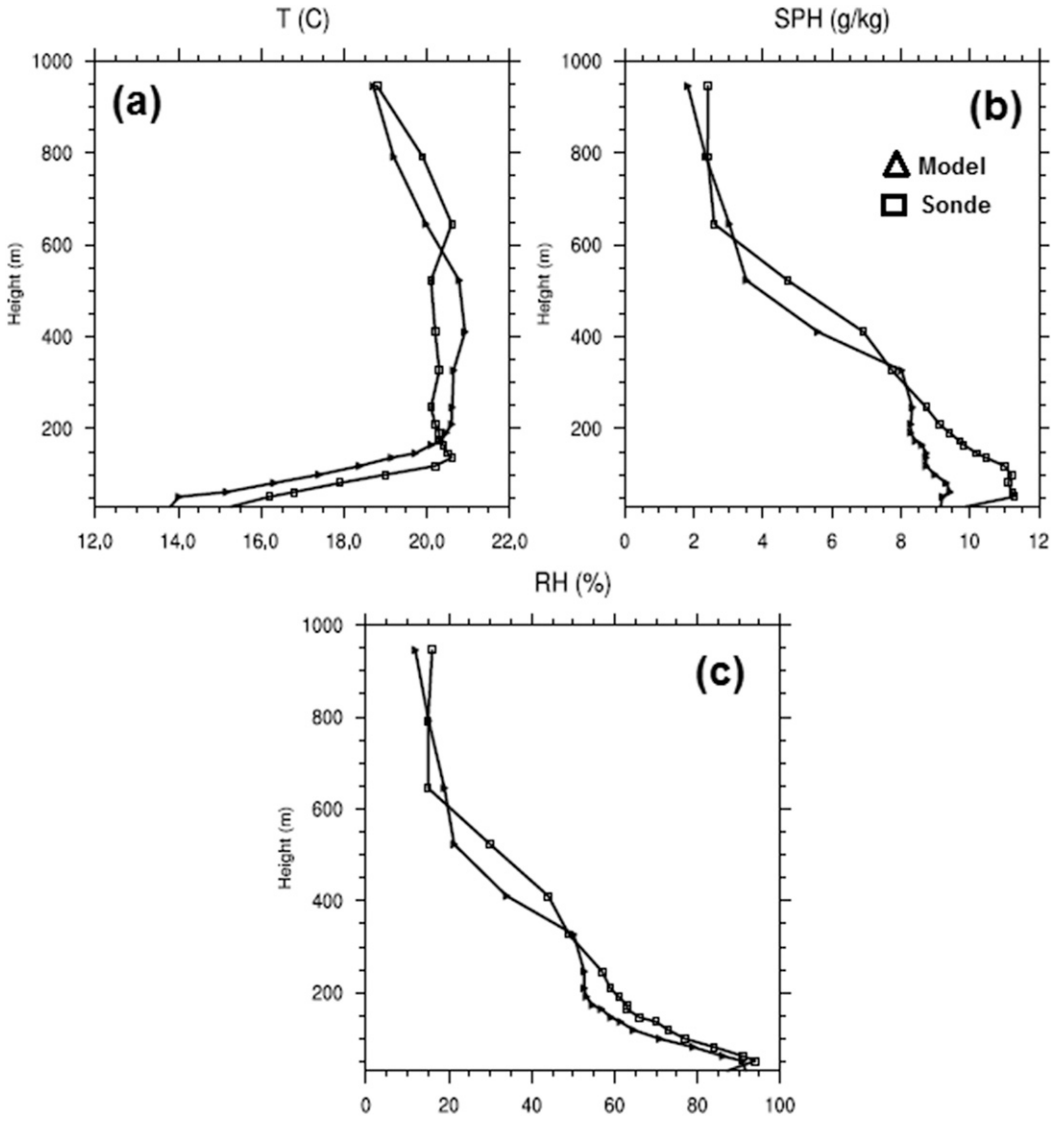

FIG. 6. Comparison between observed (line with squares) and simulated (line with triangles) profile of (a) temperature and (b) relative humidity at 0000 UTC 30 Nov 2016.

u^* during the fog events (Figs. S4a,b). However, we find that both the observed and simulated TKE and u^* increase sharply a couple of hours after sunrise, and the difference between observed and simulated TKE and u^* was larger after the sunrise. In conclusion, the WRF Model forecast for all these events demonstrates the model has skills to simulate an optimal synoptic environment for the fog formation for operational purposes.

2) FAILURE FOR DENSE FOG EVENTS

A similar comparison was conducted for the dense fog events that occurred on 8 December 2016, which model failed to simulate successfully. Figures 8a–f displays the 36-h evolution of visibility (Fig. 8a), LWC (Fig. 8b), the deviation between observed and forecasted T_2 (Fig. 8d), Ws10 (Fig. 8c), Rh_2 and Q_2 (Figs. 8e,f) for this event. Visibility evolution in Fig. 8a indicates that dense fog (Vis $<$ 200 m) onset occurred at around 2000 UTC (01:30 IST) and persisted for about 3 h. However, the model failed to produce LWC during this event. The forecast of T_2, Rh_2, and Q_2 showed warmer (Fig. 8d, a warm bias of about 1–2.5 K) and drier surface conditions throughout the fog period. This is one of the notable reasons that the model failed to predict the fog event. Figures 9a–c also compare the sounding obtained during the same dense fog event with a forecast of temperature, specific humidity, and relative humidity profile valid at 0000 UTC (0530 IST), respectively. Again this sounding

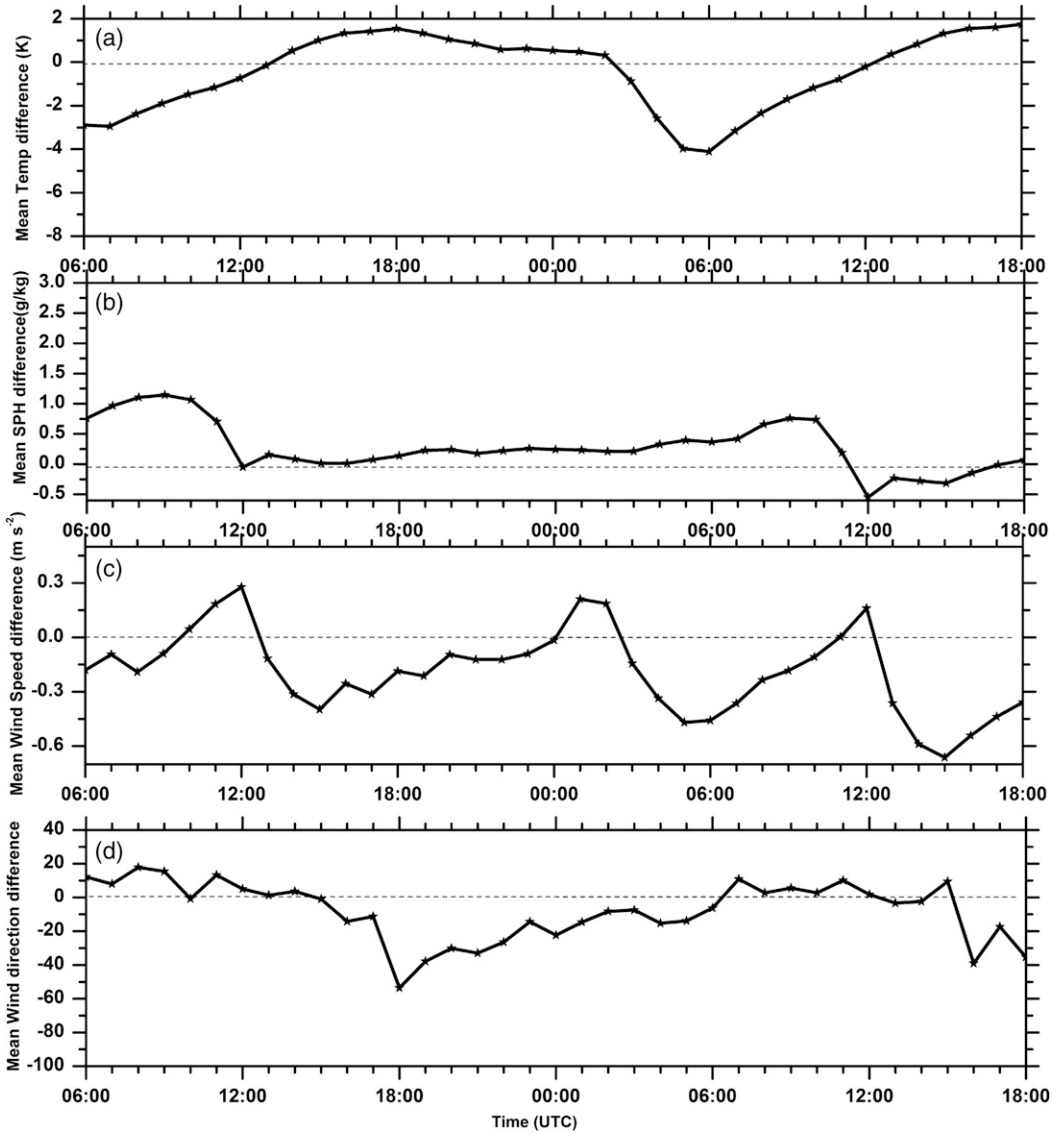

FIG. 7. Time series of the mean difference between observed and simulated (observed − simulated) (a) temperature at 2 m (T_2), (b) specific humidity at 2 m (Q_2), (c) 10-m wind speed (Ws10), and (d) 10-m wind direction (Wd10) for all predicted fog events.

represents the thermodynamical conditions during the dense fog period. Although the model and sounding both show strong surface inversion, the model was warmer by about 3 K at 200 m. The observed sounding showed saturated conditions near the surface and nearly deep moist layer vertically (Figs. 9b,c); however, the model produced much too dry conditions both at the surface and throughout the vertical levels. Composite of temperature and humidity profiles valid at 0000 UTC (0530 IST) during all the failed fog cases (in Table 3) are presented in Figs. S3c and S3d, respectively. We find that for most failed cases, real-time forecasts clearly show strong temperature inversions near the surface but produced very dry conditions between the surface and capping on the inversion layer (Fig. 9b). The underestimation of specific humidity in the inversion layer and dryer conditions above did not provide sufficient moisture to trigger the fog. Composite of deviation between observed and forecasted T_2, Q_2, Ws10, and Wd10, is illustrated in Figs. 10a–d, respectively, for all the failed fog events shown in Table 3. Again we find that in most cases, the forecasted temperature was 1–2 K higher than in observations (warm bias), especially during the dense fog period. While the near-surface atmosphere was quite moist in the observations, the humidity variation was significantly underestimated for all dense fog events.

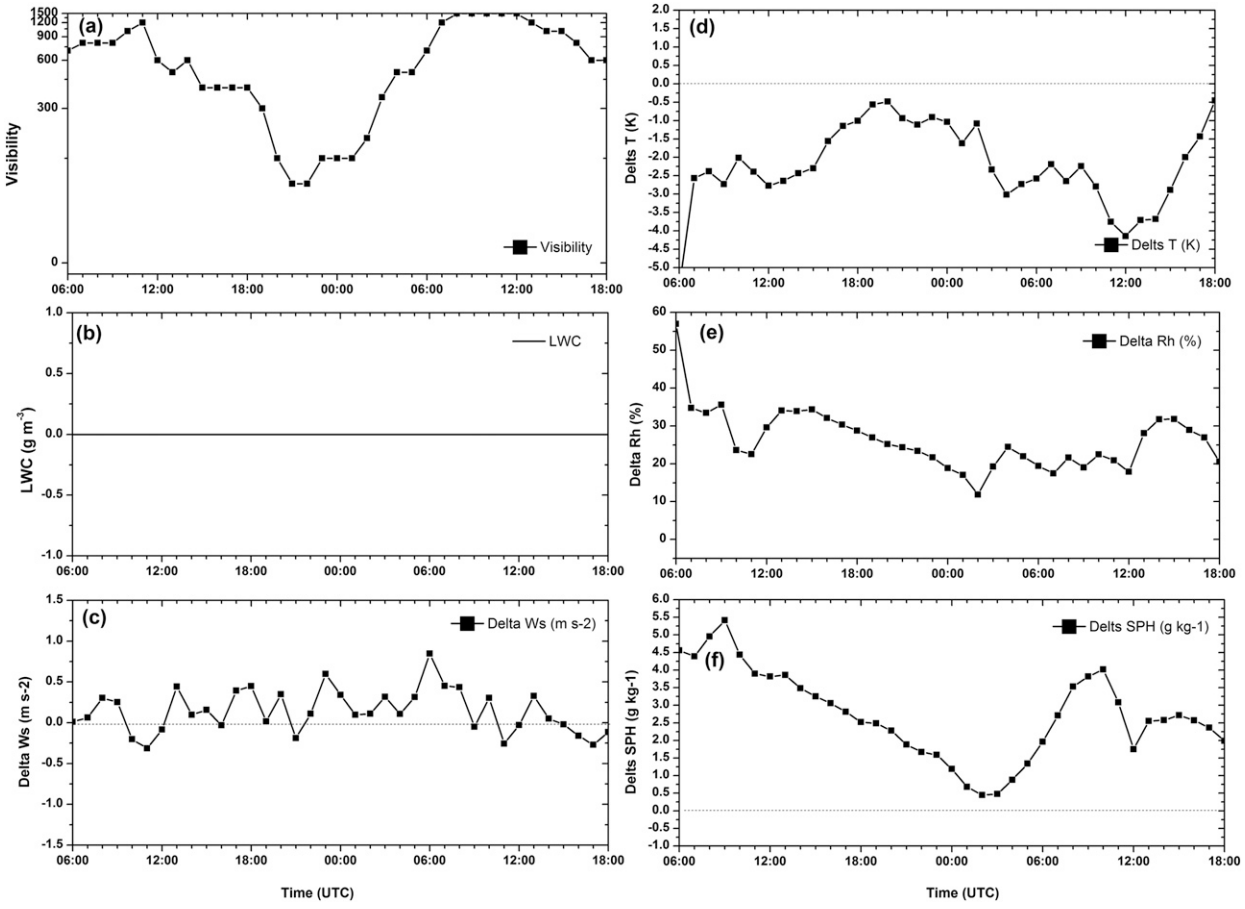

FIG. 8. Time series of (a) observed visibility (m), (b) simulated LWC ($g\,m^{-3}$), (c) difference between observed and simulated (observed − simulated) wind speed at 10 m, (d) temperature at 2 m (T_2), (e) relative humidity at 2 m (Rh_2), and (f) specific humidity at 2 m (Q_2) during 7–8 Dec 2016.

The underestimation of relative humidity (around 15%–20%) near the surface did not provide saturated conditions to cause the condensation and form fog droplets. Relative humidity depends on the temperature, and temperature biases of about 1–2 K (Fig. 10a) can introduce the bias in humidity. However, evolutions of specific humidity (Fig. 10b) show that the model showed a very dry atmosphere near the surface. For the failed event, the model simulates friction velocity u^* quite satisfactorily (Fig. S4d) but slightly underestimates TKE (Fig. S4c) during the fog event. Overall, the model failed to predict the ideal meteorological conditions during these events. We also find that on some days, the model gave a false alarm while observation did not show fog near the surface. Unlike the failed cases, the forecast showed a deeper inversion and moist atmosphere near the model levels close to the surface than the observations. Compared to observations, forecasted temperature showed cold conditions and overprediction of the moisture causing saturated conditions near the surface. With higher moisture and colder condition compared to observations, the WRF Model forecast provided a favorable surface condition for dense fog formation (please see Fig. S2) and gave a false alarm.

3) EVALUATION OF FORECASTS FOR DENSE FOG EVENTS

To assess the performance of a real-time forecast, that is, whether fog will occur or not (binary information), the hit rate (HR), false alarm ratio (FAR), missing rate (MR) and critical success index (CSI) using a contingency table (Zhou and Du 2010) were evaluated for the all deterministic dense fog events listed in Table 3. During the 2016–17 and 2017–18 winter period, 43 dense fog events (Vis $<$ 200 m) were recorded at IGI airport, out of which the real-time forecast was able to predict 29 dense fog events. On five occasions, the model gave false alarms. Table 4 presents the skill scores for dense fog events (Vis $<$ 200 m) during the 2016–18 season.

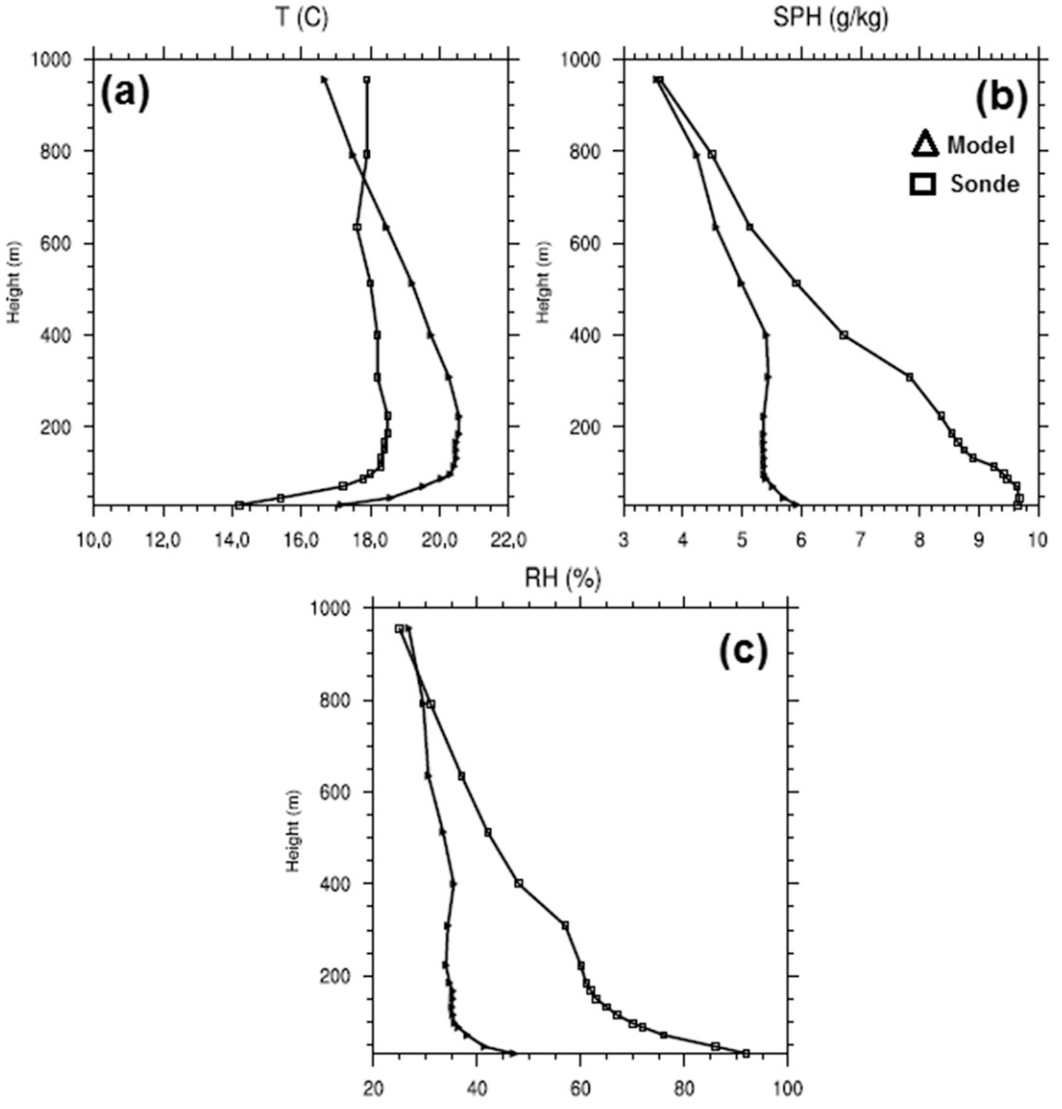

FIG. 9. Comparison between observed (line with squares) and simulated (line with triangles) profile of (a) temperature and (b) relative humidity at 0000 UTC 8 Dec 2016.

The HR indicates the percentage of correctly predicted dense fog events and nonfog events, which is the most direct measure of accuracy for the binary forecasts. The skill score for the HR and CSI is relatively promising with a value of 0.76 and 0.6, respectively. These values are higher than the median value of 0.5, which indicates that the model has reasonable good predictive accuracy in predicting the fog events correctly with respect to a total number of the observed dense fog events. FAR is quite low (0.19), and MR is also lower (0.32) than the median value of 0.5, which indicates that the performance of the real-time forecast is better for both dense fog events and no-fog events. Some of the causes of unsuccessful prediction of fog are difficulties in simulating processes like radiative cooling in the nocturnal boundary layer, low-level inversions, surface energy budget, TKE, moisture availability, synoptic advection, and synoptic-scale conditions (Gultepe et al. 2009; Zhang et al. 2013; Pu 2017; Wærsted et al. 2019; Román-Cascón et al. 2019). Apart from this, an inappropriate initial condition also plays a significant role in the unsuccessful prediction of fog (Steeneveld and Bode 2018; Pithani et al. 2019b). In the present study, we found a very dry and warm atmosphere near the surface that did not provide saturated conditions to cause condensation and form fog droplets during the failed cases. We have also seen dry bias in the initial fields (Fig. 11a) during most of the failed cases. For all the successful dense fog events, the median value of relative humidity was close to 70%, whereas it was

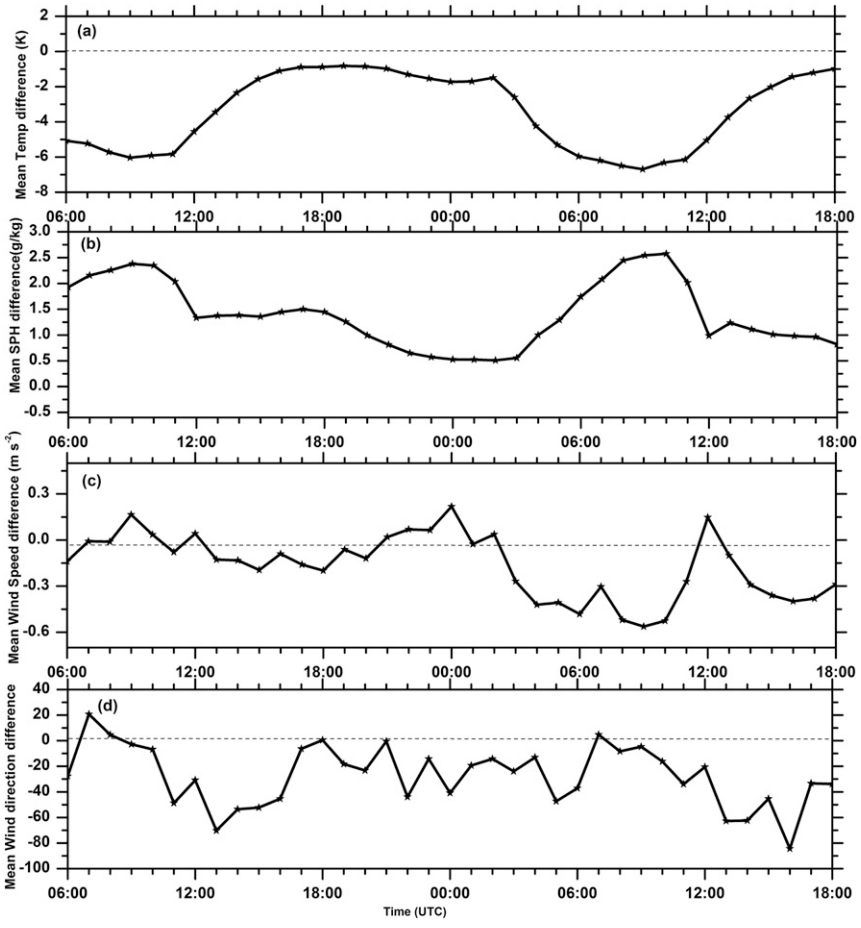

FIG. 10. Time series of the mean difference between observed and simulated (observed − simulated) (a) temperature at 2 m (T_2), (b) specific humidity at 2 m (Q_2), (c) 10-m wind speed (Ws10), and (d) 10-m wind direction (Wd10) for failed fog events.

close to 50% for all failed cases. Nevertheless, the result presented in Table 4 indicates that the skill of the real-time forecast is reasonably good in spite of challenges in accurately predicting meteorological variables near the surface. Based on our previous sensitive studies (Pithani et al. 2019a,b), we find that the MYNN2.5 PBL scheme with WSM6 microphysics combination shows better results in simulating nocturnal inversion layer, threshold values of temperature and humidity (saturated conditions) near the surface. This combination also works better in simulating LWC near the surface over the Indian region but never tested in the operational forecasting system. These studies have also shown that successful prediction of LWC not only linked to the quality of initial conditions, but the appropriate combination of PBL, radiation, microphysics, and land surface is essential for better performance of fog conditions over India. The HR (78%) demonstrated in the present study indicates that the combination of the PBL scheme. Microphysics schemes and the land surface model has the ability to simulate the optimal boundary layer environment for fog formation. Therefore, it works reasonably well for the fog cases over India in the operational forecast. This is further supported by predicted LWC, which follows the mean cycle of observed

TABLE 4. A contingency table for the number of fog cases observed vs the number of cases predicted by the WRF Model for WiFEX 2016–17 and 2017–18.

Observed	Predicted		
	Yes	No	Total
Yes	29	5	34
No	14	38	52
Total	43	43	86
False alarm rate	FAR = 5/(29 + 5) = 0.14 (14%)		
Missing rate	MR = 14/(29 + 14) = 0.32 (32%)		
Critical success index	CSI = 29/(29 + 5+14) = 0.60 (60%)		
Hit rate	HR = (29 + 38)/(86) = 0.78 (78%)		

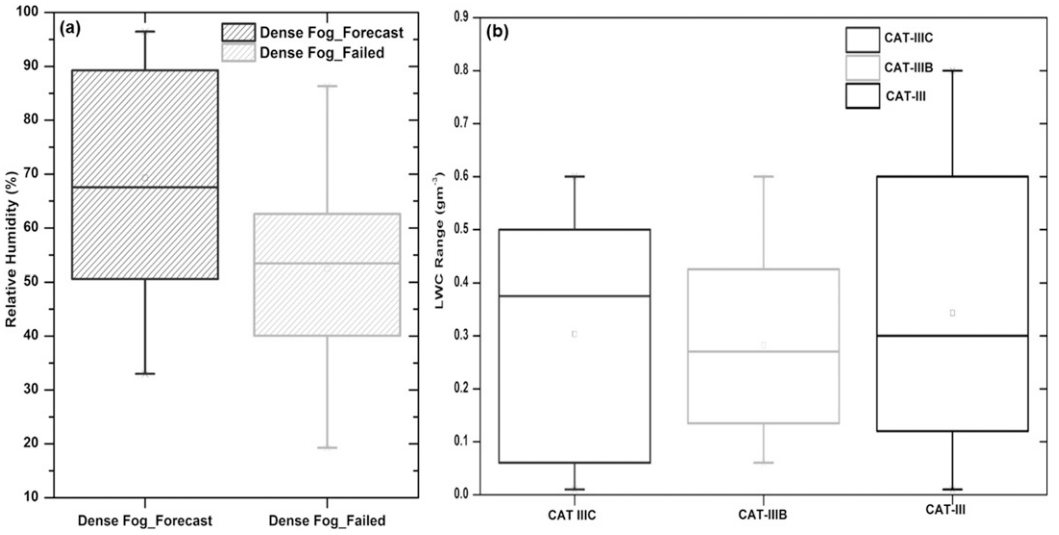

FIG. 11. (a) Box-and-whisker plot of relative humidity at the surface level from GFS IC/BC for all predicted and failed dense fog events, (b) box-and-whisker plot of predicted LWC for observed CAT-IIIC (Vis < 50 m), CAT-IIIB (Vis < 175 and >50 m), and CAT-III (Vis < 500 and >175 m) fog events predicted by the model.

LWC (Fig. 4d) and does not differ significantly with observations.

4. Discussion

The WRF Model was used to produce a real-time forecast to support the WiFEX field campaign in Delhi during the 2016–18 winter seasons. The primary objective in the present work has been to evaluate the performance of the real-time forecast against the observation of dense fog occurrences at IGI airport, New Delhi. Usually, it is challenging for the WRF Model to predict fog accurately, mainly due to large errors in the near-surface parameters such as the inversion, temperature, and humidity in the model forecast. Commonly used model lowest-level LWC has been used to validate the occurrence of fog with visibility observations. After the analysis of all the simulations over the study area, evaluation results show that the accuracy of the model forecast is dependent on the accurate prediction of temperature, humidity, depth of the inversion layer, and vertical distribution of moisture with the inversion layer. For most of the successful cases, the model accurately predicted the temperature inversion layer, moisture within the inversion layer, and threshold values of temperature and humidity (saturated conditions) near the surface, which is the optimal synoptic environment for the fog formation. The model also simulates TKE and u^* quite correctly during the fog life cycle indicating the turbulence was in an appropriate range to develop and sustain the fog. On the other hand, for most of the failed cases, the model was unable to forecast expected saturated conditions to trigger fog formation. Not many differences were observed in wind speed, the depth of the inversion layer, TKE, and u^* but the simulated profiles of temperature and relative humidity indicated a warmer and drier atmosphere at the surface and in the mixed layer compared to observations, especially in the late night and early morning hours. The Q_2 evolution (Fig. 10b) indicates that the bias in humidity was not linked to the inability of the model to forecast strong nocturnal cooling, but the model itself was drier during the failed events. A recent study by Wærsted et al. (2019) quantified the contribution of a different local process to the liquid water budget of a thick fog using the LES model. Their study indicates that profiles of humidity and temperature have a significant impact on fog development, sustainment, and dissipation. In the vertically moist atmosphere, entrainment is weak as the layer above fog is moist, and therefore the LWP is sufficient to fill the entire mixed layer. In the case of a dryer atmosphere, fog rapidly loses liquid water due to fast entrainment and can accelerate fog dissipation through mixing with dry air. In failed cases, the model difficulties of simulating enough moisture at the surface and in a mixed layer found to be the leading cause of lack of LWC near the surface.

Payra and Mohan (2014) obtained a positive temperature bias and negative moisture bias during the fog period using Lin microphysics and the ACM2 PBL scheme with a three-nested domain. They concluded that LWC is not a useful direct model output for fog forecasting over Delhi. On the other hand, Román-Cascón et al. (2012, 2016) and Pithani et al. (2019b)

showed sensitivity to the WRF single/double moment scheme with MYNN2.5 PBL and was proved to perform adequately for fog conditions. Pithani et al. (2019b) further illustrated that a single larger domain with finer resolution, more vertical levels in the boundary layer, and updated LULC using ISRO 30-s resolution produced adequate LWC during the fog conditions. The result obtained in this study with the employed configuration agrees with the previous findings of work comparing different microphysics and PBL combination (Román-Cascón et al. 2012, 2016; Pithani et al. 2019a,b) and clearly illustrates that the modeled LWC provides adequate information for fog forecasting. However, a comparison between model and observed (Fig. 4c) LWC shows that in many cases, the model tends to produce too much liquid water during the onset and mature phase of fog. These results are consistent with the previous work (Muller et al. 2010; Román-Cascón et al. 2016; Fernández-González et al. 2019). Despite the better skill, the model systematically produces a cold temperature bias during fog period for the success cases and a warm bias for the failed cases, which indicates the inability of the model to simulate real nocturnal cooling near the surface. However, positive bias (observation − model) is smaller in absolute value for the success case. On the contrary, the bias is substantially large for the failed cases. The HR (78%) for fog in this study is found to be much better than the HR (30%) reported in a recent study using the WRF Model (Román-Cascón et al. 2019). However, it should be noted that most of the success cases in the present study were related to advection fog driven by large-scale synoptic conditions (not shown) while the fog cases evaluated in the study by Román-Cascón et al. (2016) were associated with radiation fog or cloud-base lowering. Instead of using the LWC approach, Payra and Mohan (2014) obtained the HR of 95% over Delhi using a multirule diagnostic approach (based on temperature, humidity, and wind speed) using a reanalysis data, whereas, Goswami and Sarkar (2017) developed an analog dynamical model and found the HR of 79.5% for fog-induced visibility over Delhi using meteorological fields from the WRF Model.

Accurate forecast of fog often requires an accurate initial condition (Pithani et al. 2019b). It is important to consider when the model is initialized, and often error introduced early in the initial conditions shows an inability to forecast threshold values of the meteorological variables accurately. To examine the causes of error in predicted relative humidity at the surface and its sensitivity to model initial conditions, we compared the near-surface relative humidity in IITM-GFS analysis at 0000 UTC (0530 IST) for all successful and failed fog events listed in Table 3. Figure 11a shows the box-and-whisker plot of relative humidity at 0000 UTC (0530 IST) for all successful and failed dense fog events. The simulations that predicted the dense fog accurately showed more moisture at the surface in the IITM-GFS analysis at 0000 UTC (0530 IST) than the simulations that failed to predict the dense fog event. For all the successful dense fog events, the median and mean value of relative humidity distribution was close to 70%. The 25th and 75th percentile of relative humidity values were observed between 50%–90%. In contrast, for all failed dense fog events, IITM-GFS analysis at 0000 UTC (0530 IST) was much drier, causing a more significant deviation in relative humidity from the observations. As seen in Fig. 11a the median and mean value of the relative humidity distribution was close to 50% for all failed cases. The 25th and 75th percentile of relative humidity values were observed between above 40%–64%. This suggested that a better prediction of the fog is sensitive to moisture amount in the model's initial conditions. Note that the mean value of relative humidity in the IITM-GFS analysis at 0000 UTC (0530 IST) shows a clear distinction between the failed and successful cases; however, the distribution shows some overlap for the 75th percentile of relative humidity values for failed and successful fog events. This suggests that not all failed cases are related to an error in humidity at 0000 UTC (0530 IST) initial conditions. Some other factors, such as winds, the simulated depth of the inversion layer, and clouds, also play a role that leads to the model failure.

Another challenge the WRF Model faced in the real-time forecast was to predict the intensity of dense fog accurately. For safe flight operations at the airport, predicting the fog intensity is important, particularly for different categories (CAT) of visibility conditions for flight operations. Figure 10b presents a box-and-whisker plot of model-derived peak LWC for the different categories of the fog events observed at IGI airport. For very dense fog events (observed CAT-IIIC Vis < 50 m) the 25th and 75th percentiles of LWC values were observed between 0.07 and 0.5 g m^{-3}, whereas for dense fog (observed CAT-IIIB Vis < 175 and >50 m) the 25th and 75th percentiles of LWC values were observed between above 0.15 and 0.45 g m^{-3}. Also, for moderate fog (observed CAT-III Vis < 500 and >175 m) the 25th and 75th percentiles of LWC values were observed between above 0.08 and 0.6 g m^{-3}. Although the median value of LWC is a little higher for observed CAT-IIIC fog events (0.38 g m^{-3}) than CAT-IIIB fog events (0.28 g m^{-3}), peak LWC values are not accurately resolved. It shows a significant overlap between the spread of LWC values in observed CAT-IIIC, CAT-IIIB, and CAT-III fog

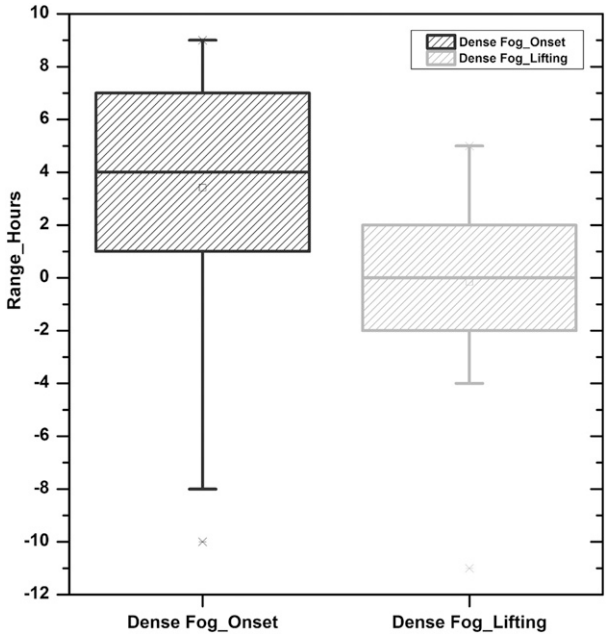

FIG. 12. Box-and-whisker plot of onset and lifting error (h) for all observed dense fog events.

events. Comparison between observed and simulated LWC for seven different dense fog events (Fig. 4) also indicate that peak value of simulated LWC is not accurately resolved by the model for different category of dense fog events. It is, therefore, challenging for the WRF Model to predict the intensity/category of fog using the LWC approach, especially for dense fog events.

Each fog type has specific onset time and duration. In addition to predicting the intensity of fog, it is also important to predict fog onset and lifting accurately for safe flight operations. Figure 12 shows the box-and-whisker plot of fog onset and fog lifting error (between predicted and observed) for the dense fog events observed at IGI airport. We find that lifting of fog is predicted relatively well by the model compared with that of predicted fog onset. For onset, the mean error was close to 4 h, while for fog lifting, it was close to zero hours. The 25th and 75th percentiles spread across the 29 dense predicted fog events for fog onset error were observed between 0 and 8 h, while the 25th and 75th percentiles of lifting error were observed between −30 min to 2 h. The onset and dissipation of fog are strongly dependent on the balance among the cooling, moisture, deposition, and turbulence during the fog life cycle. The fog is only triggered after the turbulence intensity drops below a certain level, and the air is saturated. Turbulence is more uncertain to predict in a stable layer during the early fog stage than in a well-mixed unstable layer during later fog stages (Zhou and Ferrier 2008). If the turbulence intensity inside the fog layer is smaller than the critical threshold, then fog persists. If turbulence intensity inside the fog layer increases, it starts depleting liquid water initiating the depletion effect, and when it exceeds the critical threshold, then the existing fog dissipates quickly (Zhou and Ferrier 2008; Wærsted et al. 2019). Several factors cause the turbulence intensity to exceed the critical threshold, such as a reduction in cooling at the fog top due to sunrise and increase in the local wind (Nakanishi 2000; Zhou and Ferrier 2008). We have compared TKE simulated by the model with the observed TKE at 12 m for a few fog events for which data were available (Fig. S3). We found that both the observed and simulated TKE increases a couple of hours sharply after sunrise. The difference between observed and simulated TKE was smaller during the fog event, but the difference was more significant after sunrise. Our earlier studies have shown that fog is dissipated between 0400 and 0500 UTC when model shortwave incoming radiation is above 100 W m^{-2}, and comparison of model shortwave radiation flux was better than that of the longwave radiation fluxes (Pithani et al. 2019a,b). Since sunrise is the main reason for increasing turbulence, the error in dissipation timing is small compared to the onset error. In conclusion, we see that the model can predict dense fog events with a reasonable skill (78%) using the LWC approach; however, skill for the fog onset is rather poor and calls for future work for improving onset.

5. Summary and conclusions

The primary objective in the present work was to predict fog occurrences over Delhi operationally for the WiFEX field campaign using the dynamical numerical model, WRF. Model-simulated LWC near the surface has been used for predicting fog occurrences, onset, and its lifting and was evaluated with the observational data over the IGI Airport. In total, 43 dense fog events (Vis < 200 m) were analyzed to study the performance of the operational fog forecast, success and challenges in prediction, and scope for future improvements. The skill of forecast is reliable with 78% successful prediction of the dense fog [hit rate (HR) = 0.78, false alarm (FA) = 0.15, CSI = 0.6] cases at IGI airport, suggesting that the model setup used for the operational forecast achieved physically realistic environment necessary. Particularly, it is always a challenge for the model to produce near-surface atmospheric conditions during fog episodes and accurately predict low-level inversions (Zhang et al. 2013; Massey et al. 2014; Pu 2017). However, the present study showed that the model does a good job of

producing surface atmospheric conditions at a reasonable accuracy. In spite of the good accuracy of the dense fog forecast, this study demonstrates that error in intensity and onset is large, and it is challenging to predict it with a reasonable accuracy using the LWC approach. In most of the failed fog events the model did not predict the surface variables properly (temperature and humidity) that lead to the drier conditions at the surface and within the mixed layer. It was shown that this error in moisture is associated with the error in the initial conditions. However, as indicated in this study, accurate prediction of fog occurrences, intensity, duration, and onset is still an area that needs further research in numerical models. This study can serve as a basis for future investigation of the physical factors influencing the genesis and life cycle of the fog formation at IGI Airport.

Acknowledgments. Observational data used in this study were gathered as part of the MoES-IITM-IMD collaboration, which jointly conducted the Winter Fog Experiment (WiFEX) campaign funded by MoES. The authors also acknowledge IITM Pune GFS data used in this study. All simulations and data processing were carried out on the Aditya High-Performance computing system at the Indian Institute of Tropical Meteorology (IITM), Pune, India. The funding institute for this research is MoES.

REFERENCES

Bhowmik, S. K. R., A. M. Sud, and C. Singh, 2004: Forecasting fog over Delhi—An objective method. *Mausam*, **55**, 313–322.

Biswadip, G., 2014: IRS-P6 AWiFS derived gridded land use/land cover data compatible to mesoscale models (MM5 and WRF) over Indian region. NRSC Tech. Doc. NRSC-ECSA-ACSG-OCT-2014-TR-651, 17 pp.

Collins, W. D., 2001a: Effects of enhanced shortwave absorption on coupled simulations of the tropical climate system. *J. Climate*, **14**, 1147–1165, https://doi.org/10.1175/1520-0442(2001)014<1147:EOESAO>2.0.CO;2.

——, 2001b: Parametrization of generalized cloud overlap for radiative transfer calculations in general circulation models. *J. Atmos. Sci.*, **58**, 3224–3242, https://doi.org/10.1175/1520-0469(2001)058<3224:POGCOF>2.0.CO;2.

Dimri, A. P., D. Niyogi, A. P. Barros, J. Ridley, U. C. Mohanty, T. Yasunari, and D. R. Sikka, 2015: Western disturbances: A review. *Rev. Geophys.*, **53**, 225–246, https://doi.org/10.1002/2014RG000460.

Fernández-González, S., P. Bolgiani, J. Fernández-Villares, P. González, A. García-Gil, J. C. Suárez, and A. Merino, 2019: Forecasting of poor visibility episodes in the vicinity of Tenerife Norte Airport. *Atmos. Res.*, **223**, 49–59, https://doi.org/10.1016/j.atmosres.2019.03.012.

Gautam, R., N. C. Hsu, M. Kafatos, and S.-C. Tsay, 2007: Influences of winter haze on fog/low cloud over the Indo-Gangetic plains. *J. Geophys. Res.*, **112**, D05207, https://doi.org/10.1029/2005JD007036.

Ghude, S. D., and Coauthors, 2017: Winter fog experiment over the Indo-Gangetic plains of India. *Curr. Sci.*, **112**, 767–784, https://doi.org/10.18520/cs/v112/i04/767-784.

Gilliam, R. C., and J. E. Pleim, 2010: Performance assessment of new land surface and planetary boundary layer physics in the WRF-ARW. *J. Appl. Meteor. Climatol.*, **49**, 760–774, https://doi.org/10.1175/2009JAMC2126.1.

Goswami, P., and S. Sarkar, 2017: An analogue dynamical model for forecasting fog-induced visibility: Validation over Delhi. *Meteor. Appl.*, **24**, 360–375, https://doi.org/10.1002/met.1634.

Gultepe, I., 2015: Mountain weather: Observation and modeling. *Advances in Geophysics*, Vol. 56, Academic Press, 229–312, https://doi.org/10.1016/bs.agph.2015.01.001.

——, M. Pagowski, and J. Reid, 2007: A satellite-based fog detection scheme using screen air temperature. *Wea. Forecasting*, **22**, 444–456, https://doi.org/10.1175/WAF1011.1.

——, and Coauthors, 2009: The fog remote sensing and modeling field project. *Bull. Amer. Meteor. Soc.*, **90**, 341–359, https://doi.org/10.1175/2008BAMS2354.1.

Hong, S. Y., Y. Noh, and J. Dudhia, 2006: A new vertical diffusion package with an explicit treatment of entrainment processes. *Mon. Wea. Rev.*, **134**, 2318–2341, https://doi.org/10.1175/MWR3199.1.

Jenamani, R. K., 2007: Alarming rise in fog and pollution causing a fall in maximum temperature over Delhi. *Curr. Sci.*, **93**, 314–322.

——, 2012: Development of intensity based fog climatological information system (daily and hourly) at IGI airport, New Delhi for use in fog forecasting and aviation. *Mausam*, **63**, 89–112.

Kulkarni, R. G., R. K. Jenamani, P. Pithani, M. Konwar, N. Nigam, and S. D. Ghude, 2019: Loss to aviation economy due to winter fog in New Delhi during the winter of 2011–2016. *Atmosphere*, **10**, 198, https://doi.org/10.3390/atmos10040198.

Massey, J. D., W. J. Steenburgh, S. W. Hoch, and J. C. Knievel, 2014: Sensitivity of near-surface temperature forecasts to soil properties over a sparsely vegetated dryland region. *J. Appl. Meteor. Climatol.*, **53**, 1976–1995, https://doi.org/10.1175/JAMC-D-13-0362.1.

Mitra, A. K., L. R. Meena, and R. K. Giri, 2006: Forecasting of temperature-humidity index using fuzzy logic approach. *National Conf. on Advances in Mechanical Engineering (AIME-2006)*, New Delhi, India, Jamia Millia Islamia.

Mukhopadhyay, P., and Coauthors, 2019: Performance of a very high-resolution global forecast system model (GFS T1534) at 12.5 km over the Indian region during the 2016–2017 monsoon seasons. *J. Earth Syst. Sci.*, **128**, 155, https://doi.org/10.1007/s12040-019-1186-6.

Müller, M. D., M. A. Masbou, and A. Bott, 2010: Three-dimensional fog forecasting in complex terrain. *Quart. J. Roy. Meteor. Soc.*, **136**, 2189–2202, https://doi.org/10.1002/qj.705.

Nakanishi, M., 2000: Large-eddy simulation of radiation fog. *Bound.-Layer Meteor.*, **94**, 461–493, https://doi.org/10.1023/A:1002490423389.

——, and H. Niino, 2006: An improved Mellor-Yamada level-3 model: Its numerical stability and application to a regional prediction of advection fog. *Bound.-Layer Meteor.*, **119**, 397–407, https://doi.org/10.1007/s10546-005-9030-8.

Pasricha, P. K., B. S. Gera, S. Shastri, H. K. Maini, A. B. Ghosh, M. K. Tiwari, and S. C. Garg, 2003: Role of water vapour green house effect in the forecasting of fog occurrence. *Bound.-Layer Meteor.*, **107**, 469–482, https://doi.org/10.1023/A:1022128800130.

Payra, S., and M. Mohan, 2014: Multirule based diagnostic approach for the fog predictions using WRF modelling tool. *Adv. Meteor.*, **2014**, 1–11, https://doi.org/10.1155/2014/456065.

Pithani, P., and Coauthors, 2019a: WRF model sensitivity to choice of PBL and microphysics parameterization for an advection fog event at Barkachha, rural site in the Indo-Gangetic basin, India. *Theor. Appl. Climatol.*, **136**, 1099–1113, https://doi.org/10.1007/S00704-018-2530-5.

——, and Coauthors, 2019b: WRF model prediction of a dense fog event occurred during the winter fog experiment (WIFEX). *Pure Appl. Geophys.*, **176**, 1827–1846, https://doi.org/10.1007/s00024-018-2053-0.

Pu, Z., 2017: Surface data assimilation and near-surface weather prediction over complex terrain. *Data Assimilation for Atmospheric, Oceanic and Hydrologic Applications*, S. K. Park and L. Xu, Eds., Vol. III, Springer, 219–240.

Román-Cascón, C., C. Yague, M. Sastre, G. Maqueda, F. Salamanca, and S. Viana, 2012: Observations and WRF simulations of fog events at the Spanish Northern Plateau. *Adv. Sci. Res.*, **8**, 11–18, https://doi.org/10.5194/asr-8-11-2012.

——, G. J. Steeneveld, C. Yagüe, M. Sastre, J. A. Arrillaga, and G. Maqueda, 2016: Forecasting radiation fog at climatologically contrasting sites: Evaluation of statistical methods and WRF. *Quart. J. Roy. Meteor. Soc.*, **142**, 1048–1063, https://doi.org/10.1002/QJ.2708.

——, C. Yagüe, G.-J. Steeneveld, G. Morales, J. A. Arrillaga, M. Sastre, and G. Maqueda, 2019: Radiation and cloud-base lowering fog events: Observational analysis and evaluation of WRF and HARMONIE. *Atmos. Res.*, **229**, 190–207, https://doi.org/10.1016/j.atmosres.2019.06.018.

Safai, P. D., and Coauthors, 2019: Two-way relationship between aerosols and fog: A case study at IGI airport, New Delhi. *Aerosol Air Qual. Res.*, **19**, 71–79, https://doi.org/10.4209/aaqr.2017.11.0542.

Steeneveld, G. J., and M. Bode, 2018: Unravelling the relative roles of physical processes in modelling the life cycle of a warm radiation fog. *Quart. J. Roy. Meteor. Soc.*, **144**, 1539–1554, https://doi.org/10.1002/qj.3300.

——, R. J. Ronda, and A. A. M. Holtslag, 2015: The challenge of forecasting the onset and development of radiation fog using mesoscale atmospheric models. *Bound.-Layer Meteor.*, **154**, 265–289, https://doi.org/10.1007/s10546-014-9973-8.

Syed, F. S., H. Körnich, and M. Tjernström, 2012: On the fog variability over South Asia. *Climate Dyn.*, **39**, 2993–3005, https://doi.org/10.1007/s00382-012-1414-0.

Van der Velde, I. R., G. J. Steeneveld, B. G. J. Wichers Schreur, and A. A. M. Holtslag, 2010: Modeling and forecasting the onset and duration of severe radiation fog under frost conditions. *Mon. Wea. Rev.*, **138**, 4237–4253, https://doi.org/10.1175/2010MWR3427.1.

Wærsted, E. G., M. Haeffelin, G.-J. Steeneveld, and J.-C. Dupont, 2019: Understanding the dissipation of continental fog by analysing the LWP budget using idealized LES and in situ observations. *Quart. J. Roy. Meteor. Soc.*, **145**, 784–804, https://doi.org/10.1002/qj.3465.

Zhang, H., Z. Pu, and X. Zhang, 2013: Examination of errors in near-surface temperature and wind from WRF numerical simulations in regions of complex terrain. *Wea. Forecasting*, **28**, 893–914, https://doi.org/10.1175/WAF-D-12-00109.1.

Zhou, B., and B. S. Ferrier, 2008: Asymptotic analysis of equilibrium in radiation fog. *J. Appl. Meteor. Climatol.*, **47**, 1704–1722, https://doi.org/10.1175/2007JAMC1685.1.

——, and J. Du, 2010: Fog prediction from a multimodal mesoscale ensemble prediction system. *Wea. Forecasting*, **25**, 303–322, https://doi.org/10.1175/2009WAF2222289.1.